Title
SIMULATION OF THE DEPLETION OF TWO-PHASE GEOTHERMAL RESERVOIRS

Authors
Pruess, K.
Bodvarsson, G.
Schroeder, R.C.
et al.

Publication Date
1979-08-01

To be presented at the Society of Petroleum Engineers 54th Annual Technical Conference, Las Vegas, NV, September 23-26, 1979

LBL-9606

CONF-790913--8

SIMULATION OF THE DEPLETION OF TWO-PHASE GEOTHERMAL RESERVOIRS

K. Pruess, G. Bodvarsson, R. C. Schroeder,
P. A. Witherspoon, R. Marconcini, G. Neri, and C. Ruffilli

August 1979

Prepared for the U. S. Department of Energy
under Contract W-7405-ENG-48

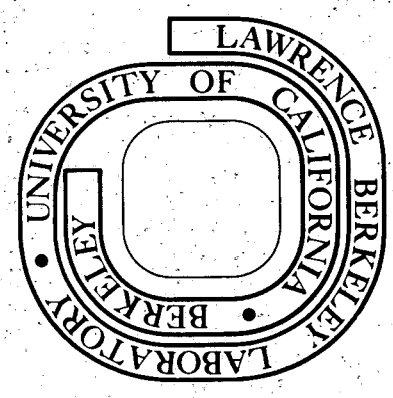

DISCLAIMER

SPE

Society of Petroleum Engineers of AIME

SPE 8266

SIMULATION OF THE DEPLETION OF TWO-PHASE GEOTHERMAL RESERVOIRS

by K. Pruess, G. Bodvarsson, R. C. Schroeder, P. A. Witherspoon, Members SPE-AIME, Lawrence Berkeley Laboratory, University of California, Berkeley, California

and R. Marconcini, G. Neri, C. Ruffilli, ENEL, Firenze, Italy

This paper was presented at the 54th Annual Fall Technical Conference and Exhibition of the Society of Petroleum Engineers of AIME, held in Las Vegas, Nevada, September 23-26, 1979. The material is subject to correction by the author. Permission to copy is restricted to an abstract of not more than 300 words. Write 6200 N. Central Expy., Dallas, Texas 75206.

ABSTRACT

The simulator SHAFT79 of Lawrence Berkeley Laboratory has been used to study the depletion of different types of geothermal reservoirs. Investigations of idealized systems include effects of gravity and fluid injection. Pressure decline is analyzed as a function of cumulative production. The main conclusions are as follows: 1) The well-known p/Z-method for estimating fluid reserves is not applicable to two-phase geothermal reservoirs. 2) There is a strong tendency towards spatially uniform boiling. This causes a pressure decline which allows in many cases estimates of the total reservoir volume and of the total heat content of the reservoir rock; 3) Propagation of a boiling front through a deep water table, as a consequence of fluid production, gives rise to a peculiar pattern of pressure decline. This may allow prediction of the distance of the water table from the producing wells and of the vertical thickness of the water zone, thereby giving important clues to estimating fluid reserves. 4) The pressure effects of injection of colder fluid depend strongly on (one- or two-) phase conditions in the reservoir, upon injection rate, and upon absolute permeability. Average pressure may actually decline in two-phase reservoirs rather than increase due to injection. Preliminary results of a case-history investigation of the Serrazzano zone at Larderello, Italy, are presented. SHAFT79 has been used for a fully three-dimensional simulation of a geologically accurate model of the Serrazzano reservoir. Comparison of computed results with field data allows improved estimates of reservoir conditions and parameters.

1. INTRODUCTION

There are only a few geothermal areas in the world where a significant portion of the in situ reservoir volume is believed to contain vapor instead of liquid.[1] Although the liquid-dominated systems are far more prevalent, the vapor-dominated systems are more readily exploitable and currently provide the major source of steam for geothermal electrical power.

Several studies have shown that most of the mass reserves of vapor-dominated reservoirs consist of liquid water.[2,3,4,5,6] This is usually concluded on the basis of the cumulative production of steam, and the corresponding pore volume that would be required if the reservoir fluid were saturated or superheated steam. The major uncertainty is not whether liquid exists in vapor-dominated systems, but whether there are significant amounts dispersed throughout the reservoir.[4] This, of course, will be site specific to some extent. With respect to the mass reserves in place, then, vapor-dominated reservoirs should more appropriately be termed "two-phase reservoirs." Liquid-dominated systems eventually develop into two-phase reservoirs after significant production has taken place. This has occurred at Wairakei, Ahuachapan, and Cerro Prieto.[7] Thus the important fundamental questions to be answered about two-phase geothermal reservoir phenemenology are applicable to all high temperature hydrothermal resources.

The present paper investigates, for a variety of idealized model reservoirs, the phenomena occuring during production from and injection into two-phase geothermal systems. Using numerical simulation and an analytically solvable lumped-parameter reservoir model, we study systems with uniform initial conditions as well as systems with steam/water interfaces. Our main objective is to identify the signature of reservoir characteristics in pressure decline curves for different production and injection strategies.

Complementing the idealized model studies is a fully three-dimensional simulation of the reservoir near Serrazzano (Italy), using a geologically accurate mesh. We report current status and results of our efforts to model 40 years of production history for this system.

2. The Simulator SHAFT79

The numerical simulations reported in the present paper were carried out with a computer program called SHAFT79. This program solves the coupled mass- and energy-transport equations for two-phase flow in a porous medium, using an integrated finite difference method. SHAFT79 is an improved version of the simulator SHAFT78, which was discussed in detail in ref. 8. The equations solved by SHAFT79 are identical to those of SHAFT78, namely:

References and illustrations at end of paper

5A

Mass transport $$\frac{\partial \phi \rho}{\partial t} = - \text{div } \underset{\sim}{F} + q \qquad (1)$$

Energy transport $$\frac{\partial U}{\partial t} = - \text{div } \underset{\sim}{G} + \tilde{Q} \qquad (2)$$

Mass flow is approximated with Darcy's law

$$\underset{\sim}{F} = \sum_{\alpha = v,\ell} \underset{\sim}{F}_{\alpha} = -\sum_{\alpha} \frac{k k_{\alpha}}{\mu_{\alpha}} \rho_{\alpha} (\nabla p - \rho_{\alpha} \underset{\sim}{g}) \qquad (3)$$

and energy flux contains conductive and convective terms:

$$\underset{\sim}{G} = - K \nabla T + \sum_{\alpha} \underset{\sim}{F}_{\alpha} h_{\alpha} \qquad (4)$$

The physical model represented by these equations involves the following assumptions and approximations: (1) Geothermal reservoirs are approximated as systems of porous rock saturated with one-component fluid in liquid and vapor form. (2) All rock properties - porosity, density, specific heat, thermal conductivity, absolute permeability - are independent of temperature, pressure, or vapor saturation; (3) Liquid, vapor, and rock matrix are in local thermodynamic equilibrium, i.e., at the same temperature and pressure, at all times; (4) Capillary pressure $p_c = p_\ell - p_v$ is neglected

For more details the reader is referred to ref. 8. The main new feature in SHAFT79 is a completely simultaneous, iterative solution of the coupled mass- and energy-transport equations. This allows between ten and one hundred times larger time steps than the sequential method employed in SHAFT78. In particular, phase transitions can be computed accurately and efficiently. SHAFT79 offers a choice of several methods for solving the coupled non-linear equations for mass- and energy-flow. The preferred solution method is fully implicit, employs a Newton/Raphson iteration for simultaneous solution of the non-linear mass- and energy-transport equations, and uses an efficient sparse solver.[9,10] SHAFT79 has been applied to problems with up to 250 elements in three dimensions. Throughputs of up to 65 per time step have been achieved with good accuracy. Here throughput is defined as ratio of the fluid mass flowing through the surface of an element, divided by the fluid mass initially in place in that element.

3. Reservoirs with Uniform Initial Conditions

The model reservoir used in the depletion studies is specified in Table 1. For the studies with uniform initial conditions it was subdivided into 20 equal sized elements with horizontal interfaces of 1 km^2 area at 50 m intervals.

Relative permeabilities were computed from a version of Corey's equations

$$k_v = \begin{cases} (2r - S)\, S^3/r^4 & \text{for } S \le r \\ 1 & \text{for } S \ge r \end{cases} \qquad (5a)$$

$$k_\ell = \begin{cases} (r - S)^4/r^4 & \text{for } S \le r \\ 0 & \text{for } S \ge r \end{cases} \qquad (5b)$$

with the residual immobile water saturation $1-r = 0.7$. Initial conditions were chosen as $T = 252\ ^{\circ}C$, $S = 0.50$ throughout the reservoir. The investigated cases (see Table 2) include production at constant flow rate as well as a somewhat more realistic production with constant external (wellbore) pressure, for which flow rates diminish with time. Various injection schemes were explored, and simulations were made for high- and low-permeability cases, with and without inclusion of gravitational forces.

3.1. Boiling Rates

Fig. 1a shows that, in many cases, the depletion process tends to give rise to a pattern of very nearly uniform boiling throughout the reservoir (cases #1, 6, 8). Only for case #2, which involves a large flow rate at low permeability, do boiling rates strongly diminish with increasing distance from the well. A higher boiling rate in some part of the reservoir causes a more rapid decline in temperature, hence in pressure. This in turn increases the flow of steam towards the region which boils more rapidly, diminishing the rate of boiling and counteracting the pressure decline associated with it. Thus there exists a negative feedback, which tends to diminish spatial variations in boiling rates upon depletion. The feedback is more effective for higher permeability. At the low permeability of 10^{-14} m^2 the feedback is still sufficiently strong to maintain constant boiling rates throughout the reservoir for the slower depletion process with constant pressure (case #8). For a high production rate of 50 kg/sec at low permeability (case #2), pressure gradients near the wellblock increase with time, as temperatures and steam densities drop. Then boiling rates near the wellblock become very large.

3.2 Pressure Decline

The well known method of extrapolating reserves in natural gas reservoirs from a plot of pressure decline vs. cumulative production (p/Z vs. Q) is based on the fact that for these systems average pressure p/Z is proportional to average density, hence proportional to reserves (see eqs. A-10, A-11). We showed in ref. 8 that this method is not applicable to geothermal reservoirs, which contain a considerable fraction of the fluid in place in the form of liquid water. For two-phase geothermal reservoirs the mechanism causing pressure decline is entirely different from that in one-phase systems. Namely, pressure declines because of heat loss and associated temperature drop in boiling, not because of mass loss. Pressure and density are independent variables in two-phase systems.

From the above it is clear that, for two-phase geothermal reservoirs, pressure decline upon production depends upon the heat capacity of the reservoir, not upon fluid reserves.

In Appendix A we present a lumped parameter model, which is an extension and improvement on a similar model in ref. 8. From eq. (A-9) we obtain, for a two-phase reservoir which produces pure steam ($h_Q = h_v$), the following approximate relationship between the total heat capacity of the reservoir rock and pressure decline dp/dQ.

$$V(1-\phi)\rho_R c_R = - \frac{1}{dp/dQ} \frac{(h_v - h_\ell)^2 \rho_v}{T + 273.15} \qquad (6)$$

Eq. (6) is applicable to two-phase reservoirs with approximately uniform initial conditions, if the depletion process is such ("slow enough") that the reservoir will stay near the limit of uniform boiling. The equation shows that the total heat capacity of the reser-

voir rock is inversely proportional to the slope of pressure decline vs. cumulative production. The proportionality factor depends only upon the average reservoir temperature. If this is known, and if the average value of volumetric rock specific heat $\rho_R c_R$ can be estimated, eq. (6) can be used to infer the total reservoir rock volume, $V(1-\phi)$. In order to estimate fluid reserves two more pieces of information are required, namely, average values for porosity and vapor saturation. Estimating fluid reserves is of crucial importance in geothermal development, and the required information can not be inferred from pressure decline curves alone.

Fig. 1b gives pressure decline curves vs. cumulative production for the cases #1, 2, 3, 4, 5, 6, 7, and 9 (see Table 2). For the cases #1, 5, 6, and 7 the depletion process conforms to the limit of uniform boiling (fig. 1a) giving rise to virtually indistinguishable decline curves for reservoirs with different permeability, with/without gravity, and different production rates. In ref. 8 we showed, that virtually indistinguishable pressure decline curves are obtained for two-phase reservoirs with the same volume but widely different porosities and mass reserves. From the slopes dp/dQ we can estimate reservoir rock volumes by using eq. (6). Table 3 shows that the estimates agree well with the actual value of .9 km^3 for our model reservoir.

From the discussion in 3.1 it should be clear why case #2 shows a different pattern of pressure decline. As depletion proceeds, boiling becomes increasingly concentrated in a region of the reservoir near the wellblock, giving rise to an acceleration of pressure decline beyond what is observed when boiling is (nearly) uniformly distributed throughout the entire reservoir volume.

The different slopes for cases #3, 4, and 9 reflect injection effects, and will be discussed in 3.3.

We have applied eq. (6) to two real systems, namely, the Serrazzano zone of the field near Larderello (Italy) and the shallow (old) zone of the Geysers. Of course, we do not know how well these systems are approximated as having uniform initial conditions, and how well the depletion process conforms to the limit of uniform boiling. Therefore, our estimates as given in Table 3 are tentative, and we do not know the error margins involved. The volume estimates should indicate some average drainage volume of the wells involved in the pressure decline analysis; they should represent lower limits for the actual reservoir volumes.

For the Serrazzano reservoir enough geological information is available to define the reservoir geometry in detail. Table 3 shows that the volume estimated from the pressure decline is only about one third of the volume of the geological mesh. There are several possible explanations for this discrepancy. (1) The distribution of temperatures, pressures, and vapor saturations may be quite non-uniform. (2) Even in regions with fairly uniform thermodynamic conditions boiling rates may show strong spatial variations. E.g., boiling rates will diminish towards the reservoir margins. (3) The observed pressure decline may be enhanced by effects of colder natural recharge. (4) Finally, there may be inaccuracies both in the estimate of pressure decline vs. cumulative production (ref. 11) and in the geometrical definition of the reservoir from geological data.

3.3 Production with Injection

In recent years, the reinjection of produced geothermal brines has received increasing attention as a possible means for (i) safe disposal, (ii) controlling subsidence, and (iii) enhancing energy recovery.[14,15,16,17] In this connection it is of great importance to understand the pressure response of a geothermal system upon injection of colder fluid. Two effects occur, namely, a pressure decrease from temperature decline, and a pressure increase near the injection well from density increase. The actual response of the reservoir depends upon how these effects balance out. If injection is made into a liquid water region, density effects upon pressure are much larger than temperature effects, and pressure will increase. A similar situation holds for injection into a superheated steam zone, as long as no two-phase zone develops near the injection well. However, injection of colder water into a two-phase zone will cause temperature and hence pressure to decline, as long as injection flow rates are low enough (reservoir permeability high enough) to maintain two-phase conditions near the injection well. Thus, injection into a two-phase zone may defeat purposes (ii) and (iii) above.

A more quantitative analysis can be made using the lumped parameter model of Appendix A. From eq. (A-9) we deduce that pressure will stay constant if fluid is uniformly injected with a specific enthalpy h_c such that

$$h_c = h_\ell - \frac{\rho_v}{\rho_\ell - \rho_v}(h_v - h_\ell) \qquad (7)$$

h_c is typically a few percent less than h_ℓ, the specific enthalpy of the saturated liquid at average reservoir temperature. Practically, the injected fluid will always have lower temperature and specific enthalpy than the water in place in the reservoir, giving rise to a pressure decline in two-phase systems.

This point is illustrated in fig. 1b. For the case with constant production rate of 50 kg/sec (#1, #3, #4) pressure declines more rapidly with injection, and more rapidly when the injection rate is increased. On the other hand, the lifespan of the reservoir is extended with injection, and more so for higher injection rate. Figs. 2a,b,c illustrate injection effects for a reservoir which is produced at constant pressure (case #9). Fig. 2a gives some saturation and temperature profiles. Under the given conditions of permeability and injection rate, water percolates down to the bottom of the reservoir quite rapidly. The injection region maintains two-phase conditions until, after 13.5 years, the reservoir has filled up from the bottom. In Figure 2b we show that, because of the pressure decline caused by injection, production flow rates drop more rapidly than in the case without injection (#6).

Thus in our examples injection slows down production, but enhances the amount of energy that can ultimately be recovered. Fig. 2c shows, as a function of time, cumulative energy production and total internal energy of the reservoir fluid for the cases #6 (no injection) and #9 (injection). In case #6 the total internal energy of the reservoir fluid diminishes as production proceeds. The amount of energy produced exceeds the energy lost by the fluid by a factor 2 - 3 reflecting a transfer of large quantities of heat from the rock to the fluid, as produced steam is replenished

by boiling in the reservoir. In the case with injection the energy content of the reservoir fluid is actually increased during production.

The pressure decline and flow rate curves for case #9 show a very peculiar irregular pattern after 24 years, corresponding to a production of $Q = 20 \times 10^6$ tons (figs. 1b and 2b). This is due to space discretization effects near a sharp steam/water interface, which emerges at this time (see fig. 2a).

4. Sharp Steam/Water Interfaces

It is not known whether sharp steam/water interfaces (SSWI) occur in geothermal reservoirs in their natural state or during exploitation.[1] If they do, it would be of very great importance to determine their location, as this would give important clues for an assessment of fluid reserves in the reservoir. Case #9 of our depletion studies in sect. 3 shows that SSWI may evolve as a consequence of cold water injection. SSWI may show their presence, among other things, in a particular pattern of pressure decline when a reservoir is depleted.

4.1. General Considerations

Numerical analysis of the phenomena occuring near a SSWI poses some difficult problems. The reason for the difficulties is that, near the interface, large gradients in various parameters can occur (e.g., pressure, saturation, boiling rate), and that parameters may vary rapidly with time. It is not clear a priori whether the spatial and time averaging implied by finite discretization will only cause a certain numerical inaccuracy, or whether it could give rise to a qualitative change in the evolution of the system. The latter appears to be a definite possibility, as the following argument shows.

In reality, water will flow upwards whenever the pressure gradient exceeds the hydrostatic head $\rho_\ell g$. If a finite space discretization is applied, however, water upflow will occur only when the average pressure gradient over a finite distance exceeds $\rho_\ell g$.

Once water does flow upwards it will flash, cooling the rock and quickly establishing a thin two-phase layer at the bottom of the steam zone. Due to the flashing both temperature and pressure will decline in this two-phase layer. This will enhance pressure gradients and will cause water upflow to increase. In a sense, water upflow feeds upon itself, so that it appears possible that systems may evolve very differently depending upon whether some small parameter change will or will not allow water upflow to get started.

Note that discretization does not affect horizontal water flow across a SSWI in such a sensitive fashion. Water will flow horizontally as soon as a non-zero horizontal component of pressure gradient exists. Numerical averaging in the horizontal direction will only affect the magnitude of water flux, whereas in the vertical case the gravitational gradient may essentially block any upflow of water.

4.2 Sustained Upflow of Water

Two regimes of flow rates can be distinguished, depending upon whether the pressure gradient required for the steam flux does or does not exceed $\rho_\ell g$. The limiting situation, for which a "sustained upflow" of water will occur, corresponds to a steam flux

$$F_{v,\,lim} = \frac{k}{\mu_v}\,\rho_v\,(\rho_\ell - \rho_v)g \qquad (8)$$

Eventually, steam saturation in the upper region of the water zone will increase such that relative permeability of steam approaches 1. Only if the applied steam flux exceeds the value given by eq. (8) will water continue to flow up. If steam flux is less than the limiting value of eq. (8) water upflow will occur only and as long as small relative permeability of steam causes larger pressure gradients to occur in the two-phase zone.

It is clear that a SSWI does not represent very difficult problems for numerical analysis in the case of "sustained upflow" of water, when average pressure gradients exceed the hydrostatic head $\rho_\ell g$. Figs. 3a through 3c present results for a reservoir as defined in Table 4 with steam flux exceeding the limiting value of eq. (8). Pressure decline at the wellblock shows characteristic bumps associated with phase transitions in subsequent elements as water moves upwards. These bumps provide a nice illustration of the effects of water injection as discussed above and in Appendix A. When water begins to enter an element (analogy to injection) boiling occurs and temperature declines. As long as steam leaves the element at a higher rate than water enters ($F_\ell/F_v<1$) density and pressure both decline. Once F_ℓ exceeds F_v, the ensuing increase in steam density causes pressure increase while temperature decline accelerates due to increased rate of boiling. Eventually, the element undergoes a transition to two-phase conditions after which pressure drops quite rapidly due to continued temperature decline in boiling. Additional computer runs show that finer discretization diminishes the amplitude of and the time interval between the pressure oscillations. The "true" response of the system, corresponding to infinite resolution, would be given by averaging over the bumps in fig. 3a.

The bumps in pressure decline and flow rate for case #9 (figs. 1b and 2b) are much more pronounced for the following reasons. (1) The spatial discretization employed in case #9 is rather coarse (25 meters vs. 1 meter in figs. 3a,b,c). (2) Phase transitions in case #9 occur towards liquid water, the pressure of which responds more sensitively than that of steam to density changes.

Fig. 3c shows the evolution of saturation profiles as the depletion proceeds. It is evident that the boiling front spreads more rapidly below the interface, into the water region, than above the interface. It is of interest to note that the saturation S at a given time is approximately constant throughout the two-phase region, while S gradually increases with time.

4.3 Slow Depletion

Our second example of SSWI involves a reservoir with parameters as defined in Table 1. Initial conditions were generated by careful gravitational equilibration of a 500 m thick steam column above a 500 m thick water column, both at $T = 252^\circ$ C. This was done in such a way as to obtain a minute pressure change across the interface between slightly superheated steam above and slightly subcooled water below. The reservoir was produced at the top at a rate of 50 kg/sec,

corresponding to a steam flux of 5×10^{-5} kg/m^{2}sec. With an initial fluid mass in place of 40.9×10^6 tons, the depletion requires 25.9 years. In order to examine discretization effects on the upflow of water, two different grids were used. The coarser grid consists of 40 elements with 25 m vertical width. In the finer grid, the two elements just above and below the interface were subdivided into three elements each, with spacings of 5 m, 5 m and 15 m. Thus there are two 5 m-elements above and below the interface respectively.

In the finer discretization water upflow quickly establishes a two-phase zone in the bottom element of the steam region (see fig. 4a). In the coarse grid, water upflow and temperature drop from boiling are not sufficient to cause a phase transition in the bottom of the steam zone. Except for this difference, both grids produce almost identical results. Minor differences in saturation profiles persist for some time, but the average pressure response is completely identical in both cases (see fig. 4a)

This agreement is somewhat surprising, and it may indicate that discretization problems at a SSWI are less severe than anticipated in our general considerations, above.

Figure 4b gives profiles of vapor saturation, flow rates and boiling rates after 5.6 years of production. These are typical for the kind of systematics which evolve before the boiling front reaches the bottom of the water region (after 6.34 years, see fig.4a). It is interesting to note that, in the top 300 m of the two-phase zone, vapor saturation decreases rather slowly with depth, while boiling rates are small and nearly constant. Near 850 m depth occurs a sudden drop in vapor saturation, which is connected with a large downflow of water, a rapidly decreasing upflow of steam, and a maximum in the rate of boiling. These peculiar phenomena are caused by the transition, near the bottom of the two-phase zone, from a small pressure gradient (slightly exceeding $\rho_v g$) to a very large pressure gradient (slightly exceeding $\rho_\ell g$), which gives rise to a convergent flow of water.

The peculiar pattern of pressure decline (see fig. 4a) can be readily understood from the boiling rate profile. Initially, pressure drops rapidly, because boiling is confined to a rather narrow two-phase zone, where it causes rapid temperature decline. As the two-phase zone spreads the decline in temperature and pressure is slowed down beyond what would result from the increased rock mass in contact with boiling water, because boiling rates are smaller near the top of the two-phase zone than near the bottom. This provides a supply of hotter steam, which flows up from depth and tends to maintain temperature and hence pressure at the top of the two-phase zone. From this results a plateau in the pressure decline curve, which extends to the time where the boiling front reaches the bottom of the reservoir. Soon thereafter pressure starts declining at a nearly constant rate, reflecting a situation of nearly uniform boiling throughout the two-phase zone. Using eq.(6) we infer, at t = 10 years, a volume of .53 km^3 for the boiling zone from the slope of pressure decline vs. cumulative production, to be compared with an actual volume of .5 km^3.

In summary, propagation of a boiling front through a deep water table gives rise to a peculiar pattern of pressure decline. This may allow identification of an impermeable basement, and to estimate volume and thickness of the boiling zone, thereby giving important information for estimating fluid reserves.

5. Simulation of the Reservoir at Serrazzano (Italy)

Serrazzano is one of the distinct zones of the extensive geothermal area near Larderello in central Tuscany.[18] Natural manifestations and utilization of steam and hot water from shallow holes in this region have occured for centuries. Deep drilling was begun after 1930, and since 1939 electric power has been generated at Serrazzano from geothermal steam. Extensive production data have been gathered over a period of forty years. Fig. 5 shows aggregate flow rates of all wells in the post-1950 period. These data as well as the detailed geological and hydrological information available make the Serrazzano zone an attractive example for developing methodology and tools for numerical simulation of geothermal reservoirs. Moreover, for environmental reasons surface disposal of produced brines is no longer acceptable in Italy, and numerical studies are needed to aid in developing an appropriate injection program.

5.1 Conceptual Model of the Serrazzano Zone, Larderello, Italy

There is an extensive body of work covering geology, geochemistry, and hydrothermal activity in the Larderello area.[18-25] This and the accumulated experience of extended geothermal development provide a conceptual model for the reservoir.[12] In brief, the Serrazzano reservoir can be characterized as a rather isolated flat inverted cup. Steam is trapped near the structural high (see fig. 6), with most of the mass reserves residing in a boiling aquifer at unknown depth, with temperature $T \gtrsim 275^o$ C. The reservoir appears bounded to the north by impermeable formations, with possible recharge areas in the southeast and southwest. High permeability zones are encountered in the densely fractured formations near the structural high.

In fig. 6 we show (labeled A to Z) the lines along which cross sections were constructed from drill logs. In Figure 7a a typical cross section is shown with the grid element locations indicated by plus signs. The solid lines are the approximate locations, respectively, of the overlying impermeable shale caprock, the carbonate/anhydrite reservoir section, and the location of the top of the basement schist. When all of the cross sections are fed into the computer program OGRE, a geologically accurate three-dimensional mesh is generated with all element volumes and surfaces accurately computed.[13] In Figure 7b a picture of the generated Serrazzano computational grid is shown in two different (rotated) views. The grid represents a reservoir that is a curved thin sheet approximately 1 km from top to bottom, and areally covers about 25 km^2. It has 234 polyhedral elements, with 679 polygonal interfaces between them. There are up to 10 interfaces per element. Element volumes range from 3.5×10^6 m^3 to 2.9×10^8 m^3, and interface areas range from .64 m^2 to 9.4×10^5 m^2.

5.2 Method of Simulation

Our first goal was to simulate the pre-exploitation phase, in order to obtain initial conditions applicable to 1939 when major production began. Using the mesh as given in fig. 7b, we started out with the entire reservoir filled with liquid water at T=275 ^{o}C,

and applied constant discharge near the structural high (elements in the N04-Z02 area in fig. 6). The simulation was continued until the temperatures at the top had dropped to 205 °C, as required by typical measured well temperatures. At this point the top 500 m of the reservoir were boiling (two-phase). While this appears reasonable in comparison with the general conceptual model, it was also evident that this approach would not allow us to model the very sizable spatial variations in temperature throughout the reservoir (some well temperatures vary as much as 80 °C over less than 1 km distance). Therefore, we (temporarily) abandoned the attempt to model the pre-exploitation phase. Instead, we began a simulation starting in January 1960, at which time a partial definition of initial conditions is available from field measurements. We intend to cover a more extensive time span once a satisfactory simulation is achieved for the post-1960 period.

Input data to be provided for the simulation include (a) reservoir parameters (geometry, rock properties), (b) initial conditions for January 1960 (distribution of temperature T, pressure p, and vapor saturation S), and (c) production flow rates at the wells. For the latter detailed and accurate field data are available. Reservoir parameters are known to some extent. Rock parameters used in the simulation are as follows: ρ_R = 2600 kg/m^3, c_R = 775 J/kg °C, K_R = 2.1 W/m °C, ϕ = 10%. Only gross features are known of the permeability distribution. The greatest uncertainty exists with regard to initial conditions. Well measurements and previous work on pressure distributions[11] provide some of the required data, but most of the initial conditions are unknown. In particular, little is known about the distribution of pore water. We begin by assuming superheated conditions near the structural high, and a rather arbitrary vapor saturation of S = 0.70 elsewhere. With this, our reservoir model contains 1.7 x 10^8 tons of water, which is close to twice the total production to date.

Determination of most of the initial conditions as well as of some other parameters is an essential part of the modeling effort. A trial-and-error process is applied, in which parameters are varied such as to reduce discrepancies between field observations (mainly temperatures and pressures) and computed reservoir behavior. A valuable criterion for appropriate parameter adjustments is that well blocks must remain very close to a steady flow situation, as pressures would change rapidly otherwise.

5.3 Present Status and Results

After a rather tedious trial-and-error procedure, we arrived at initial conditions for 1960 and permeability distributions which were consistent with the required nearly-steady flow situation in the well elements. Four zones were introduced with permeabilities ranging from 750 millidarcy near the structural high to 25 millidarcy near the reservoir margins. Table 5 shows that, after 50 days of simulation, the ratios $\dot{\rho}_n/\dot{\rho}_q$ of density changes caused by influx from neighboring elements to density changes caused by production were very close to -1 in all cases except at the well LE PRATA 4 (element C31). This enabled us to extend the simulation over a longer time period. Using time steps of 10 - 20 days, corresponding to maximum throughputs of ~ 20 for well elements, the simulation was carried out to 1400 days. The results at 720 days are not bad, indicating a steady flow situation near the wells and small changes in pressure, as required. Large pressure drops, however, occur for a number of wells after 1400 days. Fig. 8 shows mass production and simulated average steam pressure for the time from 1 January 1960 until late 1963 (1400 days later). Some imbalances in initial conditions are evident from the fact that initially average steam pressure increases. This is caused by boiling at depth, whereby additional amounts of high-temperature high-pressure steam are generated. The subsequent decline is slower by a factor of about 4 than the field observation, and is even somewhat (25%) slower than would be expected for uniform boiling. This indicates that either the rock mass in contact with boiling water should be reduced by a factor of 4, by extending the superheated zone and concentrating liquid water near the margins, or that permeability towards the reservoir margins should be reduced to concentrate boiling in a smaller area (or combinations of the two).

We plan to continue our simulation effort until a satisfactory history match up to the present time is achieved. Subsequently, we shall extrapolate the simulation into the future, examining different reinjection scenarios.

6. CONCLUSIONS

We have simulated the behavior of idealized two-phase geothermal systems under production and injection. Our numerical results, as well as an analytically solvable lumped-parameter model show that the two-phase nature of these systems determines their pressure response upon production. Systems with (nearly) uniform initial conditions show a simple behavior, which often allows to infer heat reserves and reservoir volume from pressure decline during production.

We derive a relationship between the heat capacity of the reservoir rock and the slope of pressure decline vs. cumulative production, which is verified by our numerical simulation results. It should be applicable, in an approximate way, to many natural geothermal reservoirs.

Subtle effects occur at steam/water interfaces. The propagation of a boiling front through a liquid water table, as a consequence of production from an overlying steam zone, gives rise to a peculiar pattern of pressure decline. This may give clues to an estimate of fluid reserves. We find that, even in reservoirs with large spatial variations in initial conditions, there is a strong tendency towards establishing a pattern of nearly uniform boiling throughout the two-phase zones.

Our idealized model studies are complemented by a fully 3-dimensional simulation of the highly irregular shaped reservoir near Serrazzano (Italy). We discuss methodology for developing a history match and present results for our first extended simulation covering a time period of almost four years.

Nomenclature

c_R	specific heat of rock, J/°C kg
F	mass flux, kg/m^{2}s
F_ℓ	flux of liquid, kg/m^2
F_v	flux of vapor, kg/m^2
G	energy flux, J/m^2

g	gravitational acceleration, m/s^2
h	specific enthalpy of fluid, J/kg
h_ℓ	specific enthalpy of liquid, J/kg
h_Q	specific enthalpy of produced fluid, J/kg
h_v	specific enthalpy of vapor, J/kg
K	thermal conductivity of rock/fluid mixture, J/ms^oC
K_R	thermal conductivity of rock, J/ms^oC
k	absolute permeability, m^2
k_ℓ	relative permeability of liquid, fraction
k_v	relative permeability of vapor, fraction
M	molecular weight of steam, kg
p	pressure, N/m^2
p_o	pressure at initial time, N/m^2
q, q_1, q_2	volumetric rate of mass production or injection, kg/m^3s
Q	fluid production, kg
$\tilde{Q}$	volumetric rate of energy production or injection, J/m^3s
r	parameter for relative permeability curves, dimensionless
S	volumetric vapor saturation, fraction
T	temperature, ^oC
t	time, s
t_o	initial time, s
u	specific internal energy of fluid, J/kg
U	specific volumetric energy of rock/fluid mixture, J/m^3
Z	gas compressibility, dimensionless
ρ	fluid density, kg/m^3
ρ_o	initial fluid density, kg/m^3
ρ_ℓ	density of liquid, kg/m^3
ρ_v	density of vapor, kg/m^3
ρ_α	density of phase α, kg/m^3
ρ_R	density of rock, kg/m^3
$\dot{\rho}_n$	rate of density change in well elements due to influx from neighboring elements, kg/m^3s
$\dot{\rho}_q$	rate of density change in well elements due to fluid production, kg/m^3s
μ_ℓ	viscosity of liquid, Ns/m^2
μ_v	viscosity of vapor, Ns/m^2
μ_α	viscosity of phase α, Ns/m^2
ϕ	porosity, dimensionless

Subscripts

α	liquid or vapor phase
ℓ	liquid
R	rock
ρ	referring to density
u	referring to energy
v	vapor

ACKNOWLEDGEMENT

This work was supported by the U.S. Department of Energy under contract No. W-7405-ENG-48.

REFERENCES

1. White, D.E., Muffler, L.J.P., and Truesdell, A.H.: "Vapor-Dominated Hydrothermal Systems Compared with Hot-Water Systems," Econ. Geology (1971) 66, 75-97.

2. James, R.: "Wairakei and Larderello: Geothermal Power Systems Compared," New Zealand J. Science (December 1968) 11, 706-719.

3. Ramey, H., Jr.: "A Reservoir Engineering Study of the Geysers Geothermal Field," 1969 Tax Court of the United States, 52, T.C. No. 74 (1970).

4. Sestini, G.: "Superheating of Geothermal Steam," Geothermics (1970), special issue 2, 622-648.

5. Nathenson, M.: "Some Reservoir Engineering Calculations for the Vapor-dominated System at Larderello, Italy," USGS open file report 75-142, Menlo Park, Ca. (1975).

6. Weres, O., Tsao, K., and Wood, B: "Resource, Technology and Environment at the Geysyers," Lawrence Berkeley Laboratory Report LBL-5231 (July 1977).

7. Pritchett, J.W., Rice, L.F., and Garg, S.K.: "Summary of Reservoir Engineering Data: Wairakei Geothermal Field, New Zealand," Lawrence Berkeley Laboratory Report LBL-8669 (January 1979).

8. Pruess, K., Zerzan, J.M., Schroeder, R.C., and Witherspoon, P.A.: "Description of the Three-Dimensional Two-Phase Simulator SHAFT78 for Use in Geothermal Reservoir Studies," paper SPE-7699, presented at the Fifth SPE-AIME Symposium on Reservoir Simulation, Denver, Co. January 31 - February 2, 1979.

9. Ostrowski, A.M.: Solution of Equations and Systems of Equations, Academic Press (1966).

10. Duff, I.S.: "MA28 - A Set of Fortran Subroutines for Sparse Unsymmetric Linear Equations," Report AERE-R 8730, Harwell, Oxfordshire, Great Britain (June 1977).

11. Atkinson, P.G., Miller, F.G., Marconcini, R., Neri, G., and Celati, R.: "Analysis of Reservoir Pressure and Decline Curves in Serrazzano Zone - Larderello Geothermal Field," Proc., Larderello Workshop on Geothermal Resource Assessment and Reservoir Engineering, Larderello, Italy (Sept. 12-16, 1977) 208-232.

12. Weres, O., "A Model of the Serrazzano Zone," Proc., Third Stanford Workshop on Geothermal Reservoir Engineering, Stanford, Ca. (1977) 214-219.

13. Weres, O. and Schroeder, R.C.: "Documentation for Program OGRE," Lawrence Berkeley Laboratory Report LBL-7060 (June 1978).

14. Calamai, A., Ceron, P., Ferrara, G., and Manetti, G.: "A Reinjection Experiment in the Vico 1 Well," Geothermics (1973) 2, 117-118.

15. Celati, R., McEdwards, D., Ruffilli, C., Schroeder, R.C., Weres, O., and Witherspoon, P.A.: "Study of Effect of Reinjection with a Mathematical Model," Proc., Larderello Workshop on Geothermal Resource Assessment and Reservoir Engineering, Larderello, Italy (Sept. 12-16, 1977) 308-326.

16. Cheng, P.: "Heat Transfer in Geothermal Systems," Adv. in Heat Transfer (1978) 14, 1-104.

17. Martin, J.C.: "The Replacement of Geothermal Brine as a Means of Reducing Solids Precipitation and Scale Formation," Proc., Fourth Stanford Workshop on Geothermal Reservoir Engineering, Stanford, Ca. (Dec. 13-15, 1978) 42-49.

18. ENEL (ed.): "Larderello and Monte Amiata: Electric Power by Endogenous Steam," Firenze/Italy.

19. Cataldi, R., Stefani, G., and Tongiorgi, M.: "Geology of Larderello Region (Tuscany): Contribution to the Study of the Geothermal Basins," in: Tongiorgi, E. (ed.), Nuclear Geology on Geothermal Areas, Spoleto (1963) 235-267.

20. Lazzarotto, A.: "Geologia della Zona Compresa tra l'alta Valle del Fiume Cornia ed il Torrente Pavone (Prov. di Pisa e Grosseto)," Mem. Soc. Geol. It. (1967) 6, 151.

21. Mazzanti, R.: "Geologia della Zona di Pomarance-Larderello (Prov. di Pisa)," Mem. Soc. Geol. It. (1966) 5, 105.

22. Barelli, A., Manetti, G., Celati, R., and Neri, G.: "Build-Up and Back-Pressure Tests on Italian Geothermal Wells," Proc., Second UN Symposium on the Development and Use of Geothermal Resources, San Francisco, Ca. (May 20-29, 1975), 1537-1546.

23. Celati, R., Squarci, P., Neri, G., and Perusini, P.: "An Attempt to Correlate kH Distribution with Geological Structure of Larderello Geothermal Field," Proc., First Stanford Workshop on Geothermal Reservoir Engineering, Stanford, Ca. (1975) 37-41.

24. Celati, R., Nato, P., Panichi, C., Squarci, P., and Taffi, L.: "Interactions between the Steam Reservoir and Surrounding Aquifers in the Larderello Geothermal Field," Geothermics, (1973) 2, 174-185.

25. Celati, R., Squarci, P., Taffi, L., and Stefani, G.C.: "Study of Water Levels in Larderello Region Geothermal Wells for Reconstruction of Reservoir Pressure Trend," Simposio Internacional sobre Energia Geotermica en America Latina, IILA-INDE (1976).

Appendix A: Lumped Parameter Reservoir Model for Production and Injection

We consider production from and injection into a reservoir with initial conditions and rock properties independent of position. Cumulative net fluid production is (positive for production, negative for injection)

$$Q = Q_1 + Q_2 \tag{A-1}$$

and the "effective" specific enthalpy of produced/injected fluid at time t is

$$h_Q = \frac{h_1 dQ_1 + h_2 dQ_2}{dQ_1 + dQ_2} \tag{A-2}$$

Mass and energy balance equations reduce to

$$\phi d\rho = - dQ/V \tag{A-3}$$

$$\phi d\varepsilon + (1-\phi)\rho_R c_R dT = - h_Q dQ/V \tag{A-4}$$

Expanding $d\varepsilon$ in terms of $d\rho$ and dT we obtain the slope of average temperature decline vs. cumulative production (and/or injection):

$$\frac{dT}{dQ} = \frac{(\partial\varepsilon/\partial\rho)_T - h_Q}{V\left[\phi\left(\frac{\partial\varepsilon}{\partial T}\right)_\rho + (1-\phi)\rho_R c_R\right]} \tag{A-5}$$

For some applications, e.g., if $dQ = 0$ (production and injection at the same rate), it is more useful to use time as independent variable. With the definitions

$$dQ_1 = q_1\, dt \tag{A-6a}$$

$$dQ_2 = q_2\, dt \tag{A-6b}$$

we obtain,

$$\frac{dT}{dt} = \frac{(\partial\varepsilon/\partial\rho)_T (q_1 + q_2) - (h_1 q_1 + h_2 q_2)}{V\left[\phi\left(\frac{\partial\varepsilon}{\partial T}\right)_\rho + (1-\phi)\rho_R c_R\right]} \tag{A-7}$$

For the slope of pressure decline vs. cumulative production (and/ or injection) we have from eqs. (A-3) and (A-5)

$$\frac{dp}{dQ} = \frac{(\partial\varepsilon/\partial\rho)_T - h_Q}{V\left[\phi\left(\frac{\partial\varepsilon}{\partial T}\right)_\rho + (1-\phi)\rho_R c_R\right]}\left(\frac{\partial p}{\partial T}\right)_\rho - \frac{1}{\phi V}\left(\frac{\partial p}{\partial \rho}\right)_T \tag{A-8}$$

(i) Two-phase reservoirs.

We get from eq. (A-8)

$$\frac{dp}{dQ} = \frac{\rho_v (h_Q - h_v) - \rho_\ell (h_Q - h_\ell)}{V\left[\phi\rho(\partial u/\partial T)_\rho + (1-\phi)\rho_R c_R\right]} \times \frac{\rho_\ell \rho_v}{(\rho_\ell - \rho_v)^2} \frac{(h_v - h_\ell)}{(T + 273.15)} \tag{A-9}$$

(ii) Dry steam reservoirs.

The derivatives can be computed from the gas law, $p/\rho = ZR(T + 273.15)/M$. Neglecting derivatives of the compressibility factor Z we have, approximately,

$$\frac{dp}{dQ} \approx \frac{p(u - h_Q)}{V(1-\phi)\rho_R c_R (T + 273.15)} - Z\frac{R(T + 273.15)}{V\phi M} \tag{A-10}$$

In practical cases, with ϕ considerably less than 1, the first term on the r.h.s. is negligible in comparison to the second term. Neglecting variations in Z and

T we obtain through integration the well known linear relationship between p/Z and cumulative production Q:

$$\frac{p}{Z} = \left(\frac{p}{Z}\right)_o \left(1 - \frac{Q}{V\phi\rho_o}\right) \qquad \text{(A-11)}$$

TABLE 1: RESERVOIR PARAMETERS

Rock Properties: $\rho_R = 2000$ kg/m^3
$c_R = 1232$ J/kg$^\circ$C
$K_R = 0$
$k = 10^{-13}, 10^{-14}$ m^2
$\phi = 10\%$

Reservoir Geometry: The reservoir is a vertical column of 1 km depth with a volume of 1 km^3. All boundaries are "no flow."

Table 2: Depletion Studies with Uniform Initial Conditions

Case	Production	Injection	k (m^2)	Other
#1	50 kg/sec at top of reservoir	-	10^{-13}	no gravity
#2	"	-	10^{-14}	with gravity
#3	"	50 kg/sec saturated water of T = 100 $^\circ$C at ~ 1000 m depth	10^{-13}	no gravity
#4	"	25 kg/sec saturated water of T = 100 $^\circ$C at ~ 1000 m depth	10^{-13}	no gravity
#5	with p = 10 bars at top of reservoir; initial flow rate 50 kg/sec	-	10^{-13}	no gravity
#6	"	-	10^{-13}	with gravity
#7	"	-	10^{-14}	no gravity
#8	"	-	10^{-14}	with gravity
#9	"	50 kg/sec saturated water of T = 100 $^\circ$C at -500 m depth	10^{-13}	with gravity

Table 3: Reservoir Volumes Estimated from Pressure Decline Curves

Reservoir	Pressure Decline dp/dQ (bar/kg)	Temp (°C)	Total Heat Capacity of Reservoir Rock $V(1-\phi)\rho_R c_R$ (MWyears/°C)	Total Reservoir Rock Volume $V(1-\phi)$ (km^3)
#1, after 1.3 years	-4.788×10^{-10}	250	74.4	.95
#1, after 15.2 years	-4.248×10^{-10}	234	71.2	.91
#9, after 8.2 years	$+1.202 \times 10^{-9}$	242	65.5	.84
#9, after 16.3 years	$+5.836 \times 10^{-9}$	230	56.4	.72
#4, after 2.5 years	-1.160×10^{-9}	249	71.7	.92
Big Geysers (Shallow Zone)	-1.22×10^{-11} (ref. 3)	250	2915	46
Serrazzano	-1.89×10^{-10} (ref. 11)	218	132	2.1
Serrazzano	(geologically accurate mesh)[12,13]	218	396	6.2

TABLE 4: RESERVOIR WITH SUSTAINED UPFLOW OF WATER

Rock Properties: $\rho_R = 2650$ kg/m^3
$c_R = 710$ J/kg°C
$K_R = 1.83$ W/m°C
$k = 10^{-13}$ m^2
$\phi = 20\%$

Reservoir Geometry: The reservoir is a vertical column of 30 m depth and 1 m^2 horizontal cross section. It was subdivided into 30 equal sized elements with horizontal interfaces at 1m spacing. All outer boundaries are "no flow."

Initial Conditions: The top 20 m of the reservoir contain superheated steam, and the bottom 10 m, subcooled water, both at a temperature T = 200 °C, with pressures carefully equilibrated under gravity.

Production: The reservoir was produced from the top element at a constant rate of 6.8×10^{-4} kg/sec, corresponding to a depletion within 30 days.

Relative permeabilities were computed from eqs. 5a,b with a residual immobile water saturation of $1-r = 0.35$.

Table 5: Flowing Wells in the Serrazzano Reservoir

Well	Producing Since	Location	50 Days Flow Rate (kg/sec)	50 Days $\dot{\rho}_n/\dot{\rho}_q$	50 Days p (bars)	720 Days $\dot{\rho}_n/\dot{\rho}_q$	720 Days p (bars)	1400 Days $\dot{\rho}_n/\dot{\rho}_q$	1400 Days p (bars)
Conserva	1940	PO2	4.25	- .9990	5.3	- 1.0016	5.2	- .9804	1.9
Capanna	1940	PO3	6.14	- .9988	5.7	- 1.00081	6.3	- .9920	3.7
Avalle 2	1950								
BCF3	1943	A03	4.86	- 1.0026	9.9	- .99942	9.4	- .9893	7.7
Soff. 1	1950	E03	5.19	- 1.00017	5.9	- 1.00098	4.9	- .9917	2.6
Cioccaia	1954	Z02	7.47	- .9978	7.2	- 1.0018	6.8	- .9978	8.0
#8	1957	Y03	3.36	- 1.0058	8.0	- .999936	8.5	- .9933	5.5
Pozzaie 2	1958	N04	16.36	- .99962	6.2	- 1.00018	5.9	- 1.00036	4.8
Le Prata 4	1959	C31	7.94	- 1.14	8.7	- 1.0026	9.0	- 1.0137	9.1
Le Vasche	1959	G03	5.50	- .99982	5.9	- 1.0015	5.5	- .9914	3.7
Oliveta	1961	C03			8.3	- 1.0027	6.9	- .9750	5.2
VC 2	1963	C07			10.7		13.0	- 1.4387	14.3
VC 5	1963	R38			17.1		18.8	- .6004	19.0
VC 10	1963	E08			38.6		41.6	- .8422	40.5
Campoaiperi	1965	S40			8.0		10.3		12.4
Vignacce	1966	G04			10.5		10.0		9.3
Grottitana	1968	D06			13.7		16.7		18.8
Capriola	1970	B08			23.1		22.0		21.2
Lustignano	1970	P12			22.1		23.3		22.1

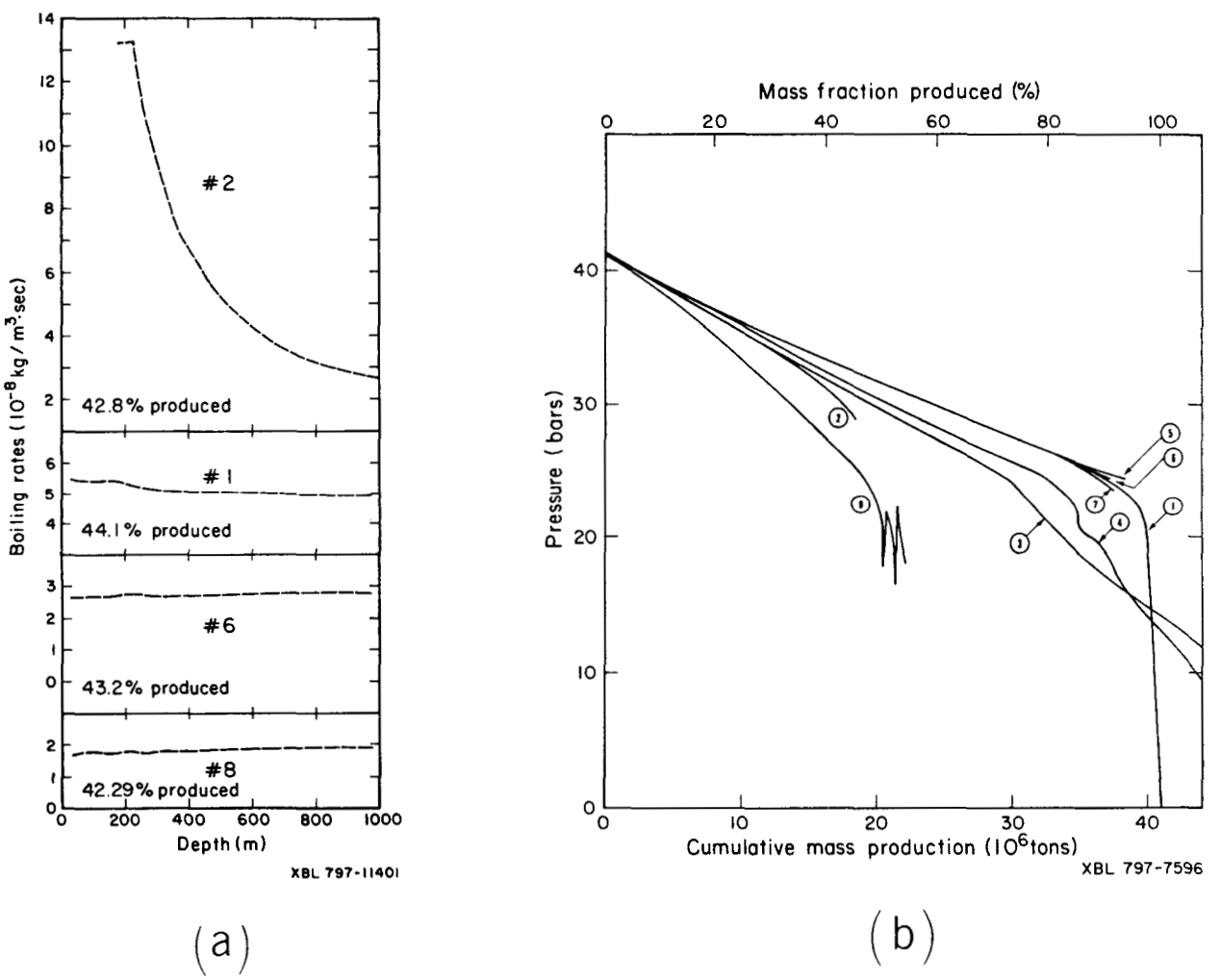

Fig. 1: Boiling Rate Profiles (a) and Pressure Decline Curves (b) during Depletion of Various Two-Phase Reservoirs. The examples shown are defined in Tables 1 and 2.

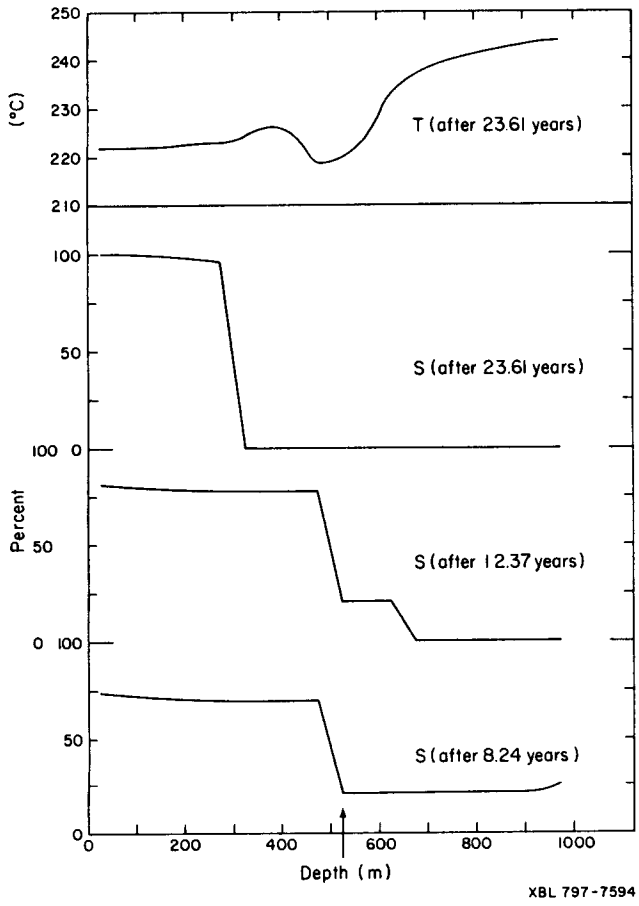

(a)

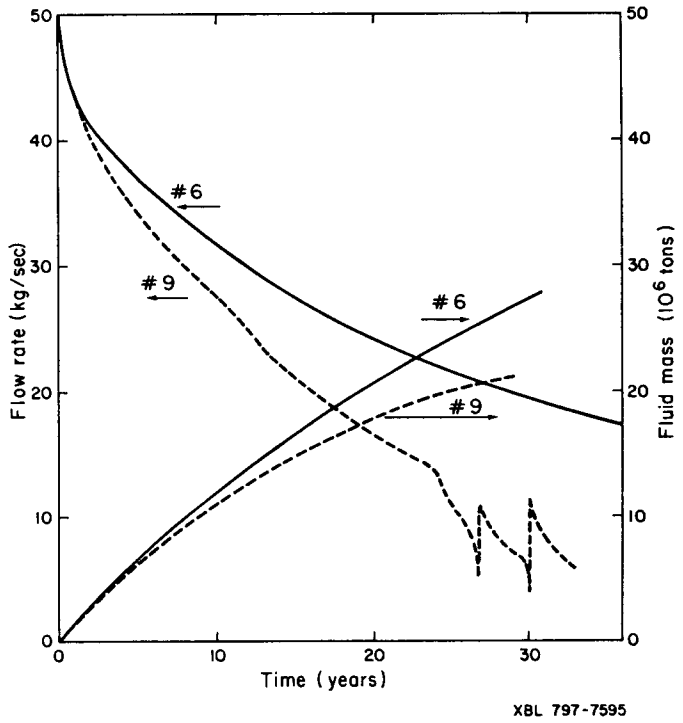

(b)

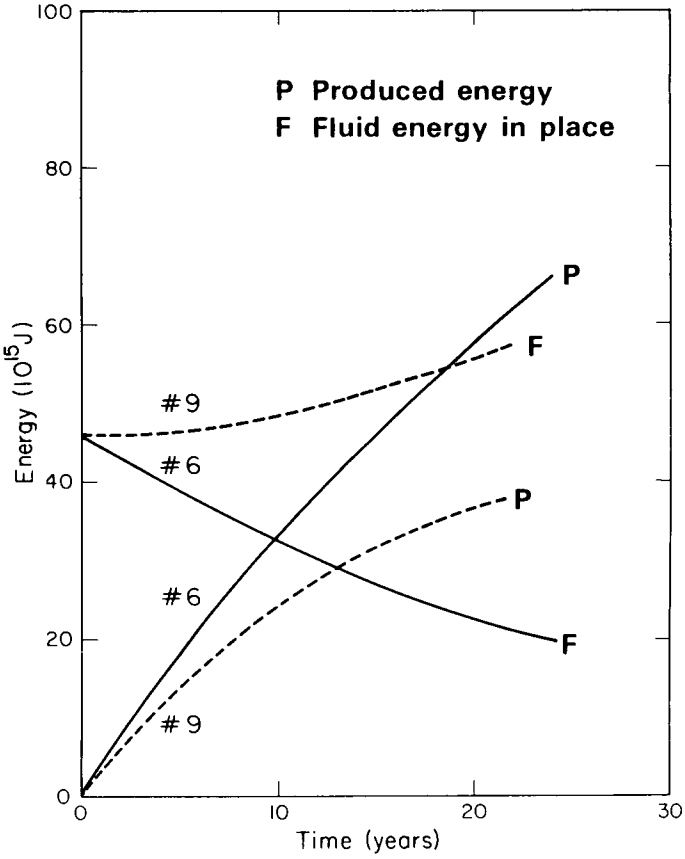

(c)

Fig. 2: Effects of Injection of Cold Water in a Producing Two-Phase Reservoir. (a) Saturation and temperature profiles for case #9 (Table 2); (b) flow rates and cumulative production with (#9) and without (#6) injection; (c) energy production and energy content of reservoir fluid.

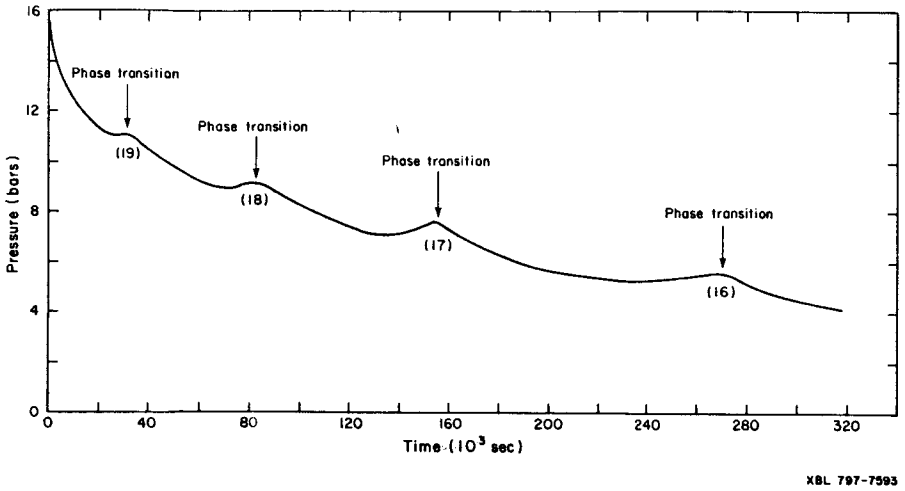

(a)

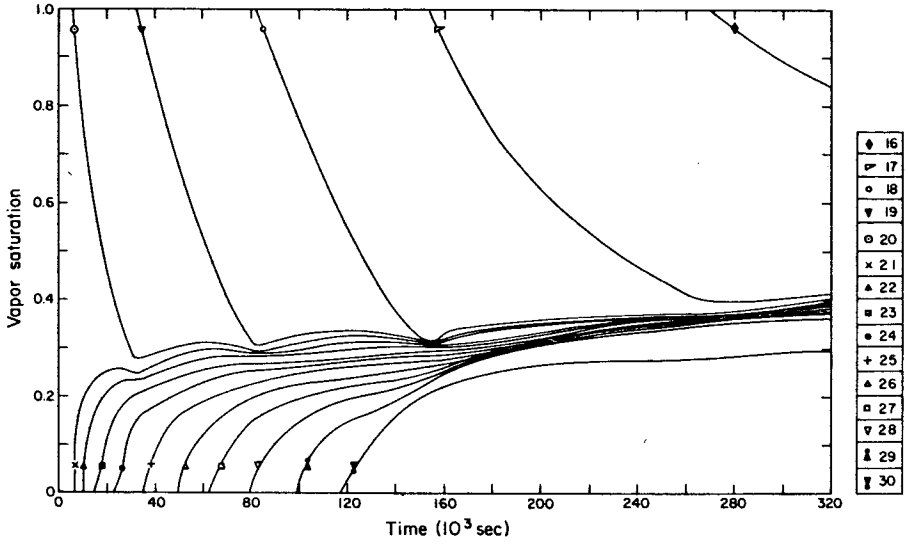

(c)

XBL 797-11403

(b)

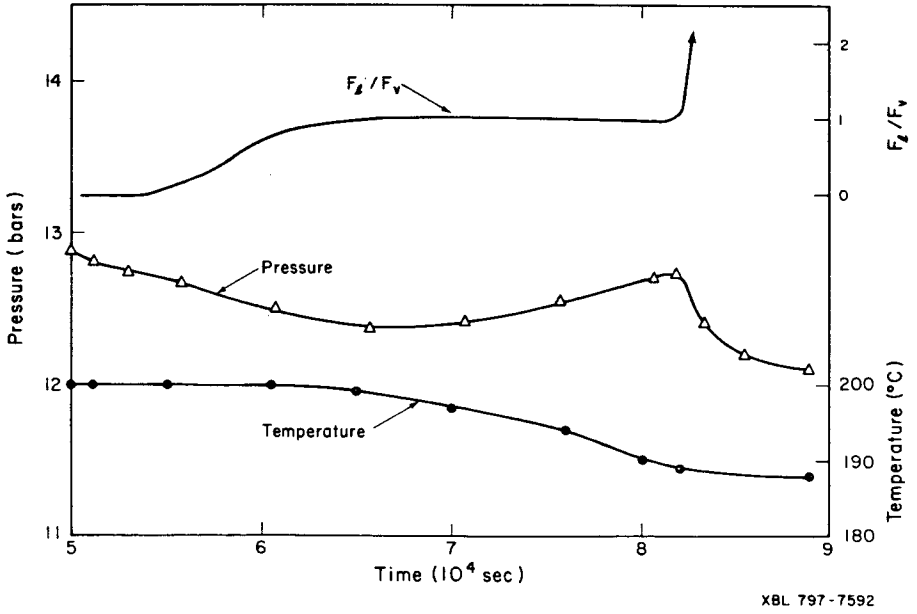

Fig. 3: Fast Depletion of a Reservoir with Sharp Steam/Water Interface. The problem is defined in Table 4. (a) Pressure in well-block; (b) parameter changes in element 18 during phase transition; (c) saturation profiles.

(a)

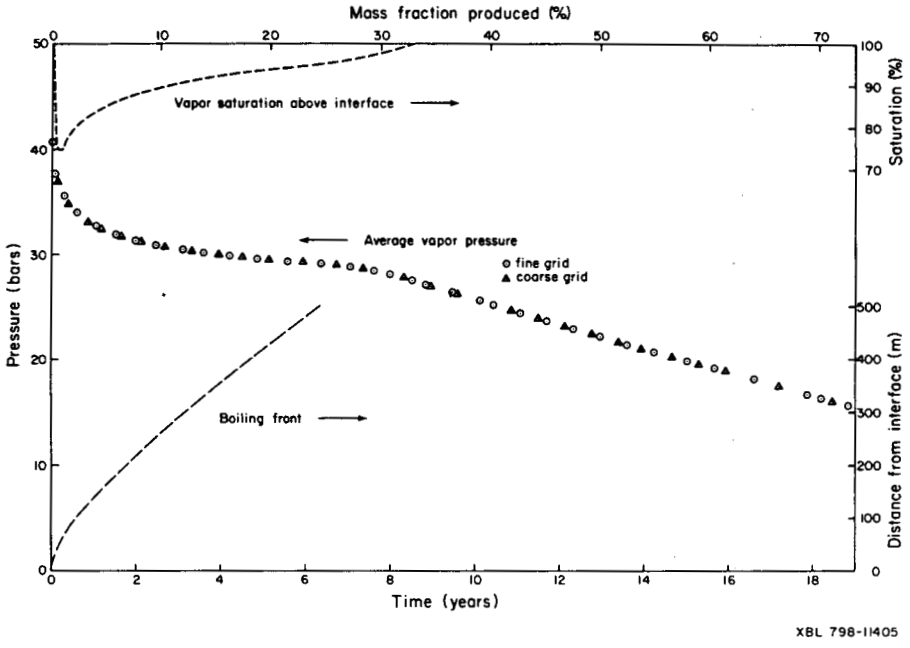

Fig. 4: Slow Depletion of a Reservoir with Sharp Steam/Water Interface. Reservoir parameters are given in Table 1. (a) Time evolution; (b) vertical profiles.

(b)

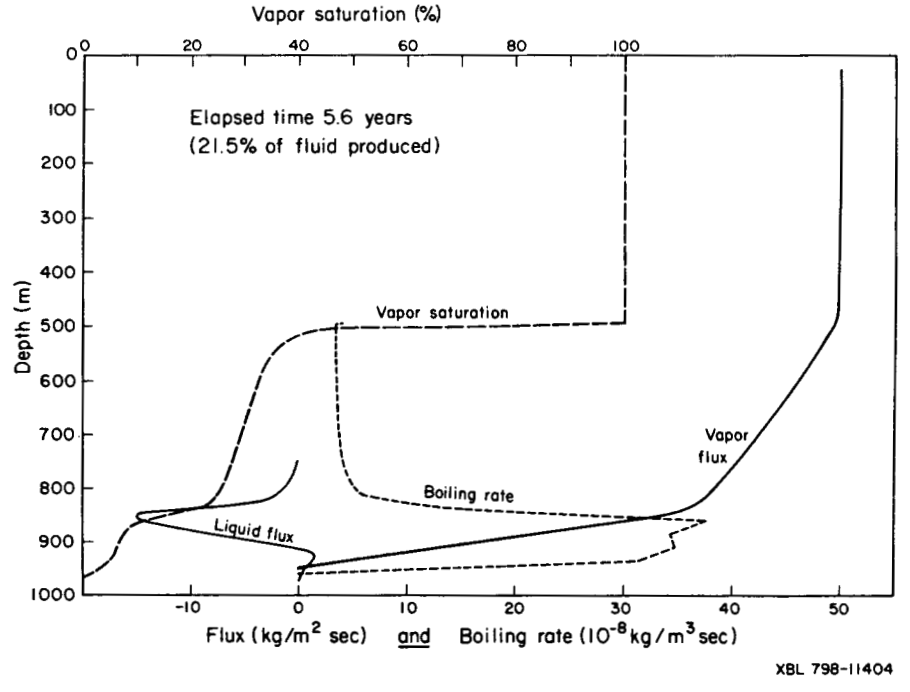

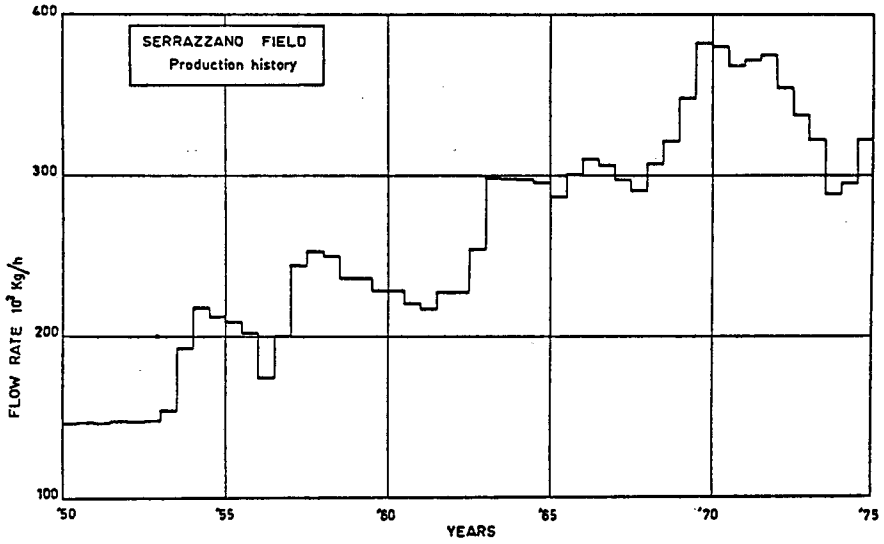

Fig. 5:
Aggregated Production Rates as Measured for the Serrazzano Geothermal Reservoir.

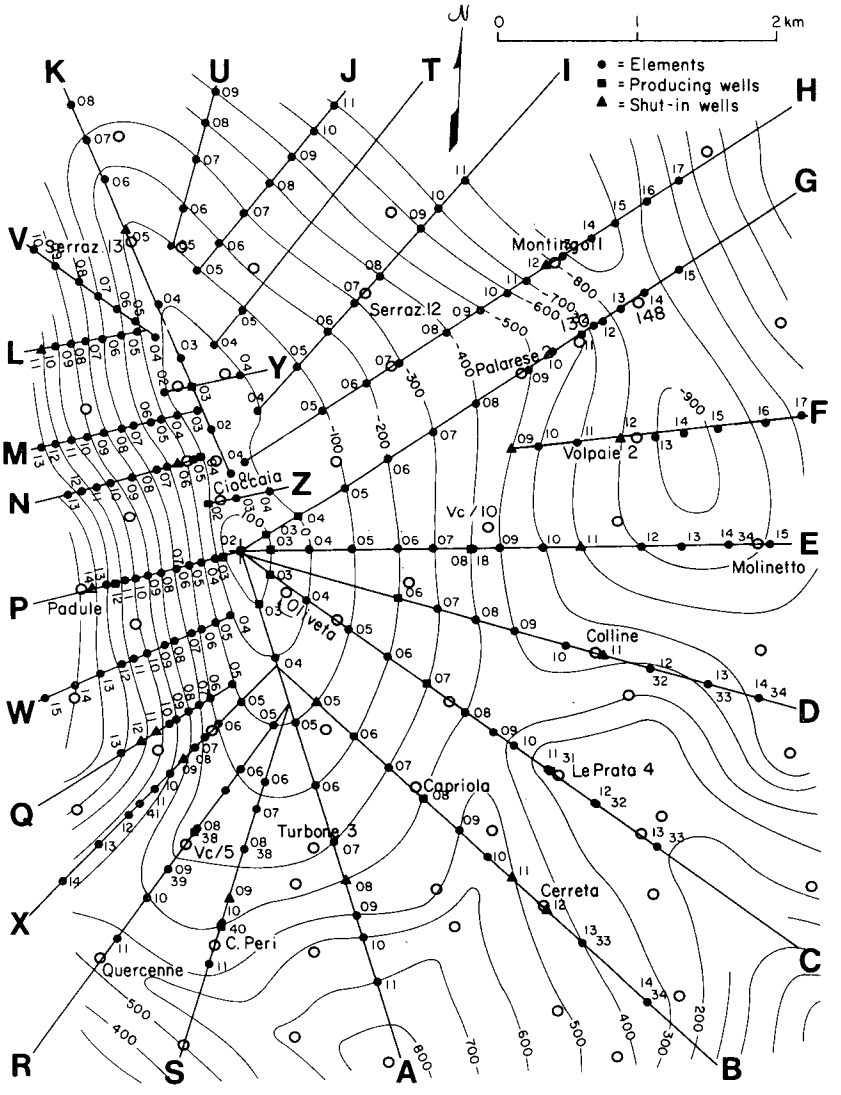

XBL 797-7591A

Fig. 6:
Caprock Elevations and Geological Cross Sections for Serrazzano.

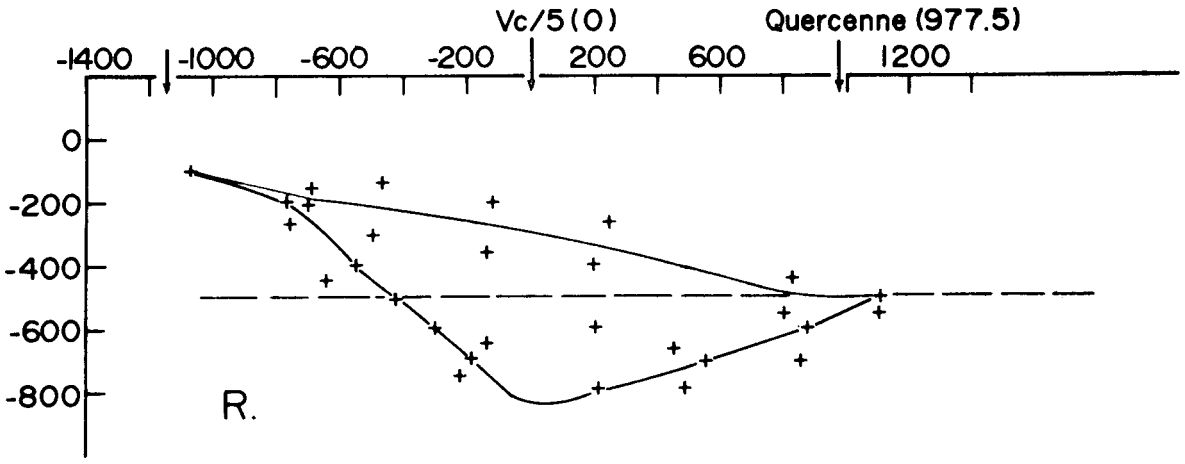

XBL 784-8202

(a)

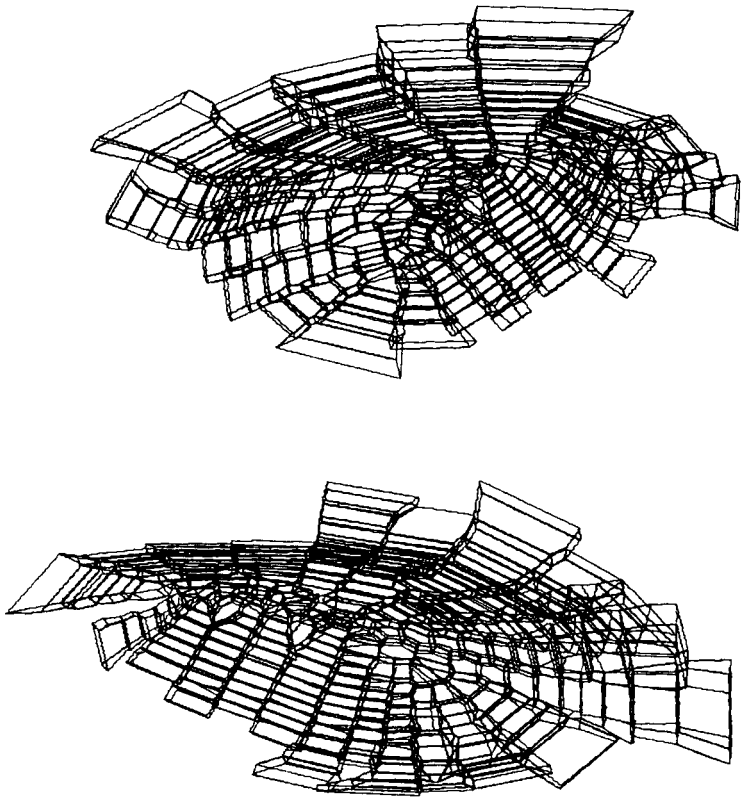

(b)

XBL 787-9570

Fig. 7:
Serrazzano Grid. (a) Typical Cross Section; (b) rotated perspective views of entire grid.

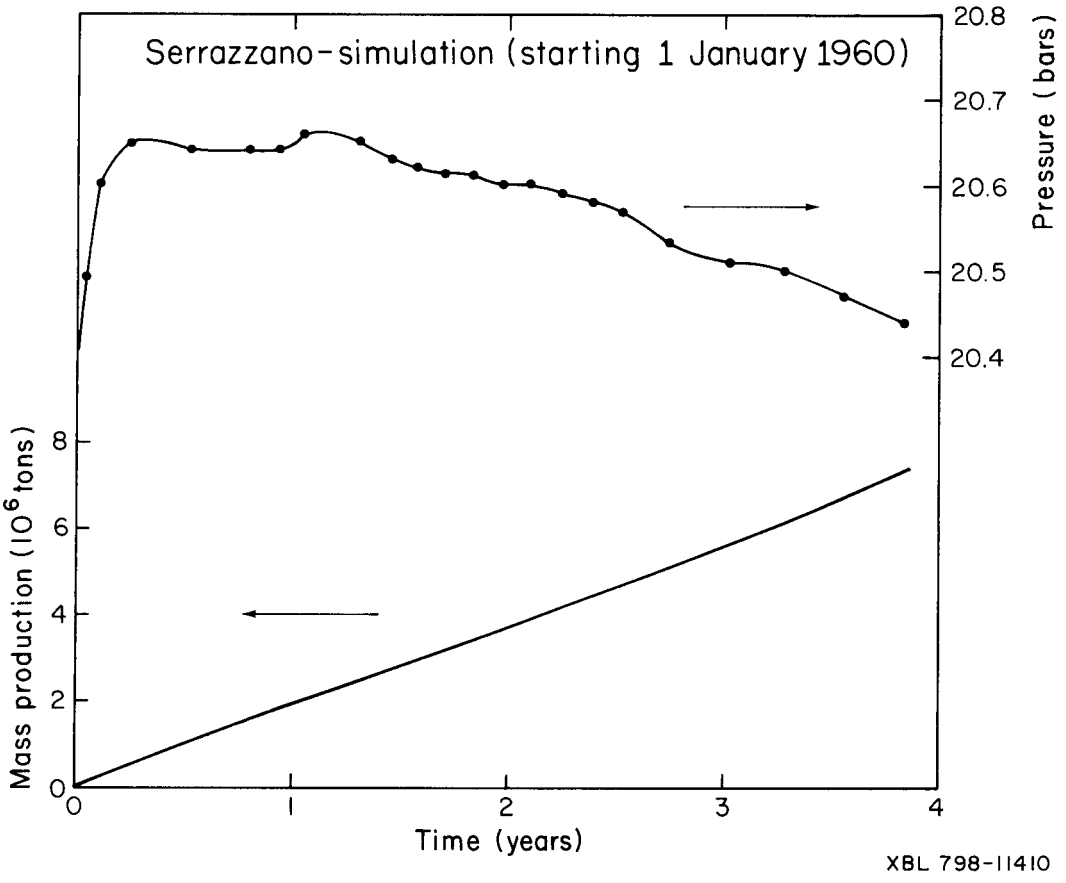

Fig. 8: Average Reservoir Steam Pressure and Cumulative Fluid Production as Calculated in Serrazzano Simulation.

TECHNICAL INFORMATION DEPARTMENT
LAWRENCE BERKELEY LABORATORY
UNIVERSITY OF CALIFORNIA
BERKELEY, CALIFORNIA 94720